A general framework for the assessment of solar fuels technologies

Supporting information

Jeffrey A. Herron, Jiyong Kim, Aniruddha A. Upadhye, George W. Huber, Christos T. Maravelias*

Department of Chemical and Biological Engineering, University of Wisconsin – Madison, Madison, WI 53706, USA

*corresponding author: Tel.: +1 608 265 9026; Fax: +1 608 262 5494. E-mail address: maravelias@wisc.edu

Additional background material

Solar PV Efficiencies

Figure S1 shows the time-evolution of photovoltaic research-cell efficiencies as compiled by NREL.

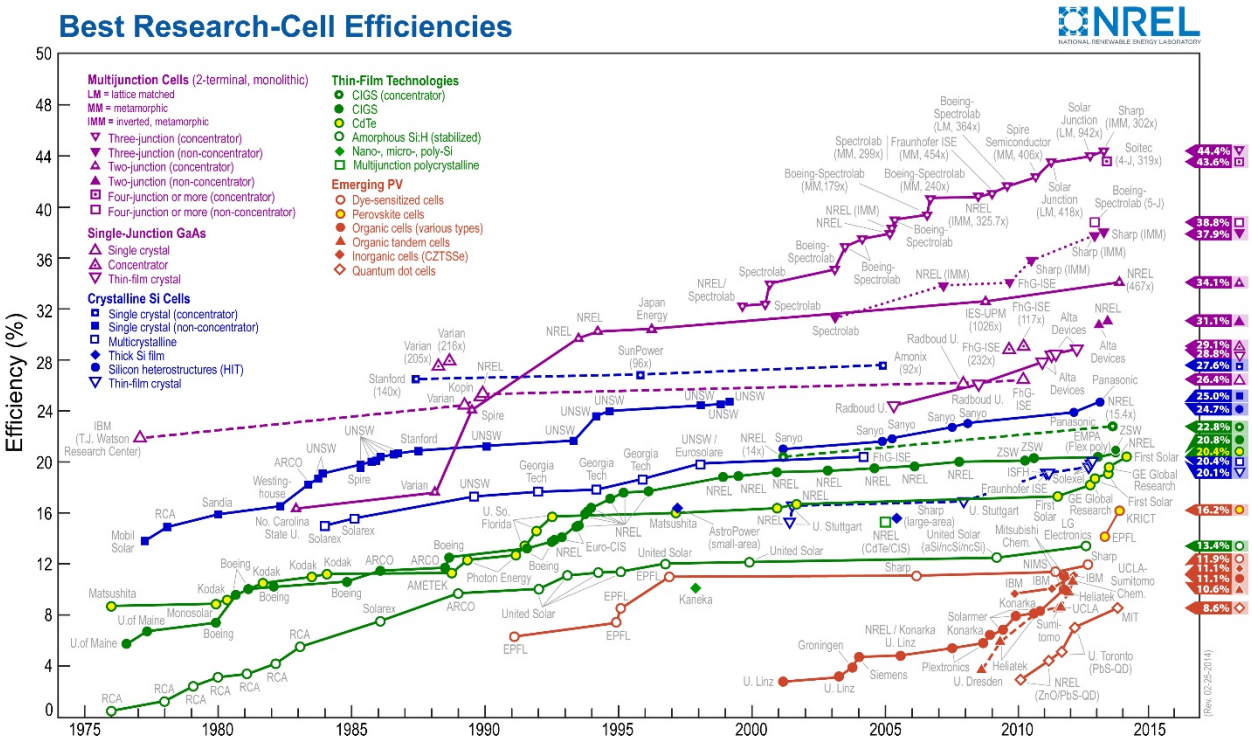

Figure S1. *Best Research cell efficiencies reported for photovoltaics by National Renewable Energy Laboratory (NREL). The chart "Best Research-Cell Efficiencies" is reprinted with permission by the National Renewable Energy Laboratory, http://www.nrel.gov/ncpv/images/efficiency_chart.jpg, Accessed June 11, 2014.*

Photo-catalytic reactors for solar fuels

Apart from mass transfer, heat transfer and kinetic considerations, the design of photo-catalytic reactors must consider radiation transfer[1]. For effective design of photo-catalytic systems for solar applications, all of the catalyst needs to be illuminated to achieve maximum output from the process. Designs for photo-catalytic reactor systems for solar application have been reviewed[2]. Various types of photocatalytic reactors such as parabolic trough reactors[3], double skin sheet photoreactors[4], optical fiber photoreactors[5], and fluidized bed photoreactors[6] have been discussed in the literature. The selection of the type of photo-catalytic reactor for a particular process depends upon the operating parameters such as temperature, pressure, throughput, etc. For a photo-catalytic system without any electrical input, packed bed reactors with compounding parabolic trough reflectors are one of the most mature and scalable technologies.

Solid adsorbents for CO_2 capture

Zeolites are microporous crystalline aluminosilicates composed of SiO_4 and AlO_4 groups. Substitution of an AlO_4 groups with a SiO_4 groups creates a negative charge, which is compensated by a cation (e.g. alkali) in the pores. Zeolite 13X has been employed in commercial hydrogen production to separate H_2/CO_2 using pressure swing adsorption.[7] Overall, zeolites have high CO_2 capacity near ambient temperature and they are very stable with respect to regeneration. However, there are significant disadvantages. In particular, at increased temperature (> 373 K), the adsorption capacity drops significantly, and the selectivity is low because water in flue gas streams will compete with adsorption sites, lowering its efficacy.

An emerging class of adsorbents are metal-organic frameworks, microporous crystalline networks composed of metal centers which are connected by organic ligands.[8, 9] MOFs can be produced of a wide variety of structures. As such, they can separate through several different mechanisms, including chemisorption, size-exclusion, and molecular sieving. Overall, MOFs are advantageous due to their stability, high surface area, large void volumes, and tenability to be tuned. A recent subset of MOFs called zeolitic imidazole frameworks (ZIFs), where metal atoms are linked by ditopic imidazolate ($C_3N_2H_3^-$)[10], have demonstrated very high selectivity for CO_2 in flue gases and high capacity.

Another class of solid adsorbents are supported amines, which function similarly as solvent amines.[11] There are many methods of supporting the amines: polymeric amines can be physically loaded into the support[12, 13], they can be covalently linked the support[14-16], or by *in situ* polymerization of aminopolymers.[12, 17] The density of the amines on the support has shown to be an important parameter in their functionality. Overall, supported amines demonstrate reasonable capacity, yet lower regeneration costs than their solvent counterparts.

Metal oxides (e.g. CaO, MgO) capture and release CO_2 through reversible, carbonate looping. One of the most common materials for carbonate looping is CaO, which forms $CaCO_3$ between 600-650°C in the presence of CO_2 and calcines to regenerate CaO between 800-850°C:[18-20]

$$CaO + CO_2 \leftrightarrow CaCO_3 \qquad \Delta H° = -179.2\ kJ/mol$$

Carbonate looping is an advantageous CO_2 capture method because the materials are abundant and low-cost. Unfortunately, the stability of these materials over many cycles is low.

Finally, hydrotalcites are a class of anionic clays with the stoichiometry $M^{2+}_{1-x}M^{3+}_{x}(OH)_2A^{m-}_{x/m}\bullet yH_2O$, where M^{2+} is typically Mg^{2+}, Zn^{2+}, or Ni^{2+}; M^{3+} is typically Al^{3+}, Ga^{3+}, Fe^{3+}, or Mn^{3+}; and A^{m-} includes CO_3^{2-}, Cl^-, SO_4^{2-}, NO_3^-. Adsorption of CO_2 occurs on the basic surface sites. Compared with metal oxides, they have lower energy costs for regeneration and retain their capacity after cycling, though they have lower capacity.[21]

Water Electrolysis Chemistry

Alkaline: At the cathode of alkaline electrolyzers, water is introduced that decomposes to form hydroxyl ions and hydrogen. The hydroxyl ions travel through the electrolyte to the anode where oxygen is evolved. The half-cell reactions are:

Cathode: $2H_2O + 2e^- \rightarrow H_2 + 2OH^-$
Anode: $4OH^- \rightarrow O_2 + 2H_2O + 4e^-$

PEM: Unlike alkaline electrolyzers, water is introduced at the anode where it is decomposed into protons and oxygen gas. The protons travel through the Nafion membrane where they are reduced to hydrogen gas at the cathode. The half-cell reactions are:

Cathode: $2H^+ + 2e^- \rightarrow H_2$
Anode: $2H_2O \rightarrow O_2 + 4H^+ + 4e^-$

Solid Oxide: In solid oxide electrolyzers, steam is fed to the cathode, where it is decomposed to hydrogen gas and oxygen ions. The oxygen ions are transported through the electrolyte where they evolve oxygen at the anode. The half-cell reactions are:

Cathode: $H_2O + 2e^- \rightarrow H_2 + O^{2-}$
Anode: $2O^{2-} \rightarrow O_2 + 4e^-$

Additional analysis material

Process flow diagram for modified CAMERE process

In Figure S2 we present the detailed process flow diagram for the modified CAMERE process, excluding the CO_2 capture and H_2 production steps. The process unit operations were optimized to minimize energy consumption and maximize yield of methanol.

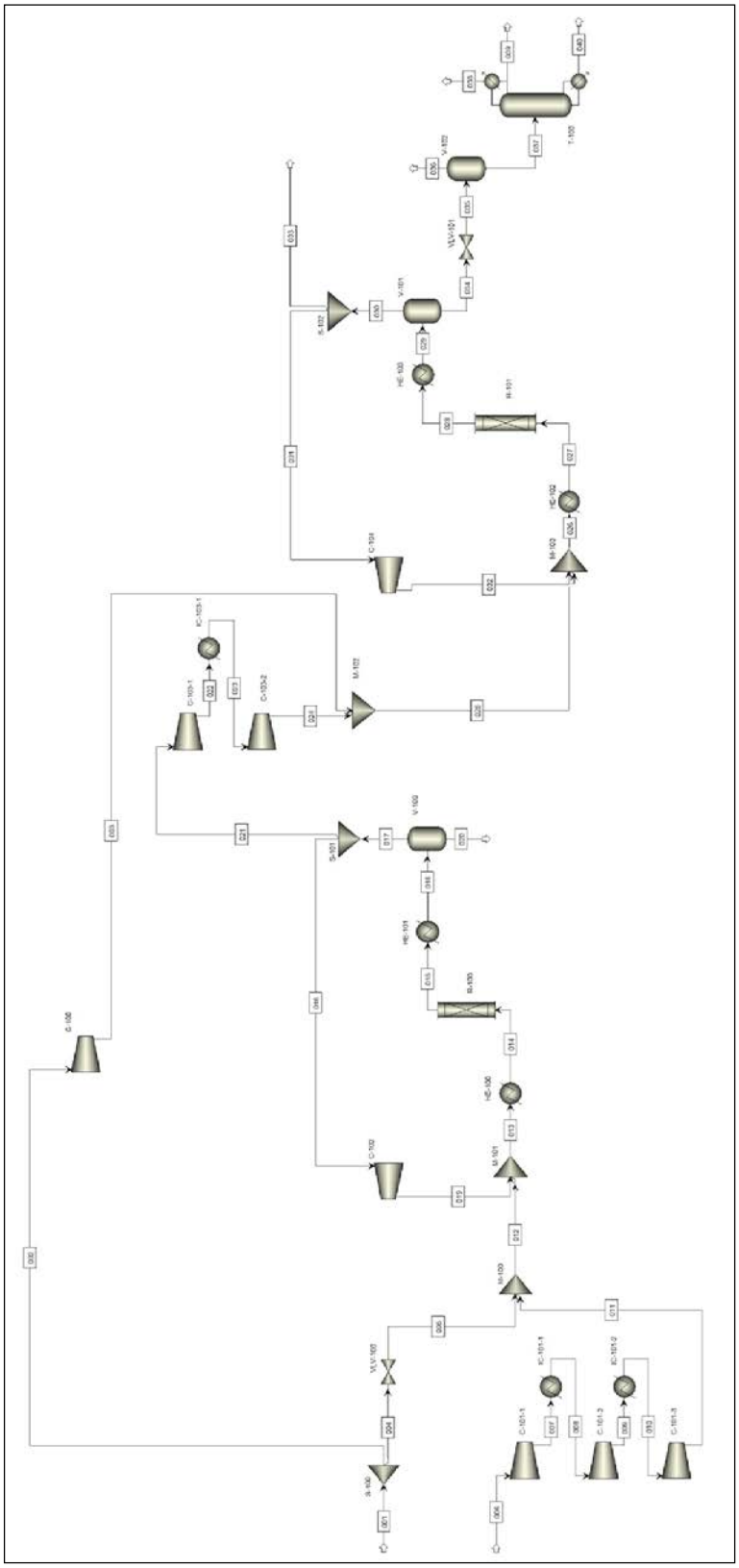

Figure S2. Process flow diagram for modified CAMERE process (excluding CO_2 capture and H_2 production steps)

Block flow diagrams for CO_2 reduction case studies

In Figure S3, block flow diagrams for the three generic CO_2 reduction case-studies are presented. In Case I, CO_2 is captured from the dilute flue gas stream via MEA absorption and transported to the solar refinery. The CO_2 stream is mixed with water and heated to 50°C before entering the photo-reactor. In the solar-reactor, CO_2 and H_2O are converted using solar energy to methanol, methane and O_2. A series of flash tanks operating from 3 to 20 atm separate the vapor (CO_2, O_2, CH_4) from the condensables (CH_3OH, H_2O). The $CO_2/O_2/CH_4$ stream is vented, while the methanol is purified to 99.8% purity using a series of distillation columns with the water recycled (please see supporting information for more details). In Case II, the process is generally the same as Case I, except that unreacted CO_2 is recovered and recycled back to the solar reactor. The concentrated CO_2 in the vapor stream is separated by physical absorption using Selexol™[22, 23] and recycled to the solar-reactor. The CH_4/O_2 stream is vented. Finally, Case III is the same as Case II except that the initial CO_2 capture occurs from an oxy-combustion process through physical absorption using Selexol™.

Process design for Gas/Liquid Separation sub-system (C)

The product of the CO_2 Reduction sub-system is sent to the Gas/Liquid Separation sub-system to separate the vapor product(s) and light gases from the liquid product(s) and water. For the specific case studied, CO_2, O_2, and CH_4 are separated from CH_3OH and H_2O, in this system. Specific details for this system are provided hereafter (with process flow diagram shown in Figure S4), optimized for a single case study. The product (1) enters an ambient pressure/temperature flash tank to recover the majority of the methanol and water (LIQUID-1), which is sent to the Liquid Product Purification sub-system. The light components are compressed to 5 atm to remove some of the residual water and methanol from the stream. The remaining lights are compressed to 22 atm and then sent through a series of flash tanks which operate at decreasing pressures to recover additional methanol and water. The light gases from each of these flash tanks are combined (GASOUT) and sent to the Gas Product Purification sub-system. The recovered methanol and water is sent to a distillation column which removes CO_2, which is dissolved in the stream. This stream (LIQUID-2) is also sent to the Liquid Product Purification sub-system.

The majority of the energy expenditures for this sub-system, as designed, are in the two compressors (there are minimal energy expenditures in the cooler and distillation column). Therefore, the energy of this system was calculated to be proportional to the mass of the light components (CO_2, O_2, and CH_4) which are compressed from near ambient to 22 atm.

Process design for Liquid Product Purification sub-system (E)

The product of the Gas/Liquid Separation sub-system is sent to the Liquid Product Purification sub-system to purify the liquid product(s) to the appropriate levels and remove any solvents or unreacted components for recycling. For the specific case studied, methanol is the only product and it is separated from H2O (which is both a solvent and reactant). The process flow diagram for this specific system is shown in Figure S5. The liquid streams from the Gas/Liquid Separation system are combined and CO_2 is purged by flashing. The remaining liquid is sent through a series

of three distillation columns which (1) remove the majority of the water, (2) remove residual water, and (3) remove any remaining CO_2.

The energy cost of this system was calculated by varying the methanol weight fraction in the incoming stream. The calculated heating duty required as a function of methanol weight fraction is shown in Figure S6. A power law was fit to the data as shown.

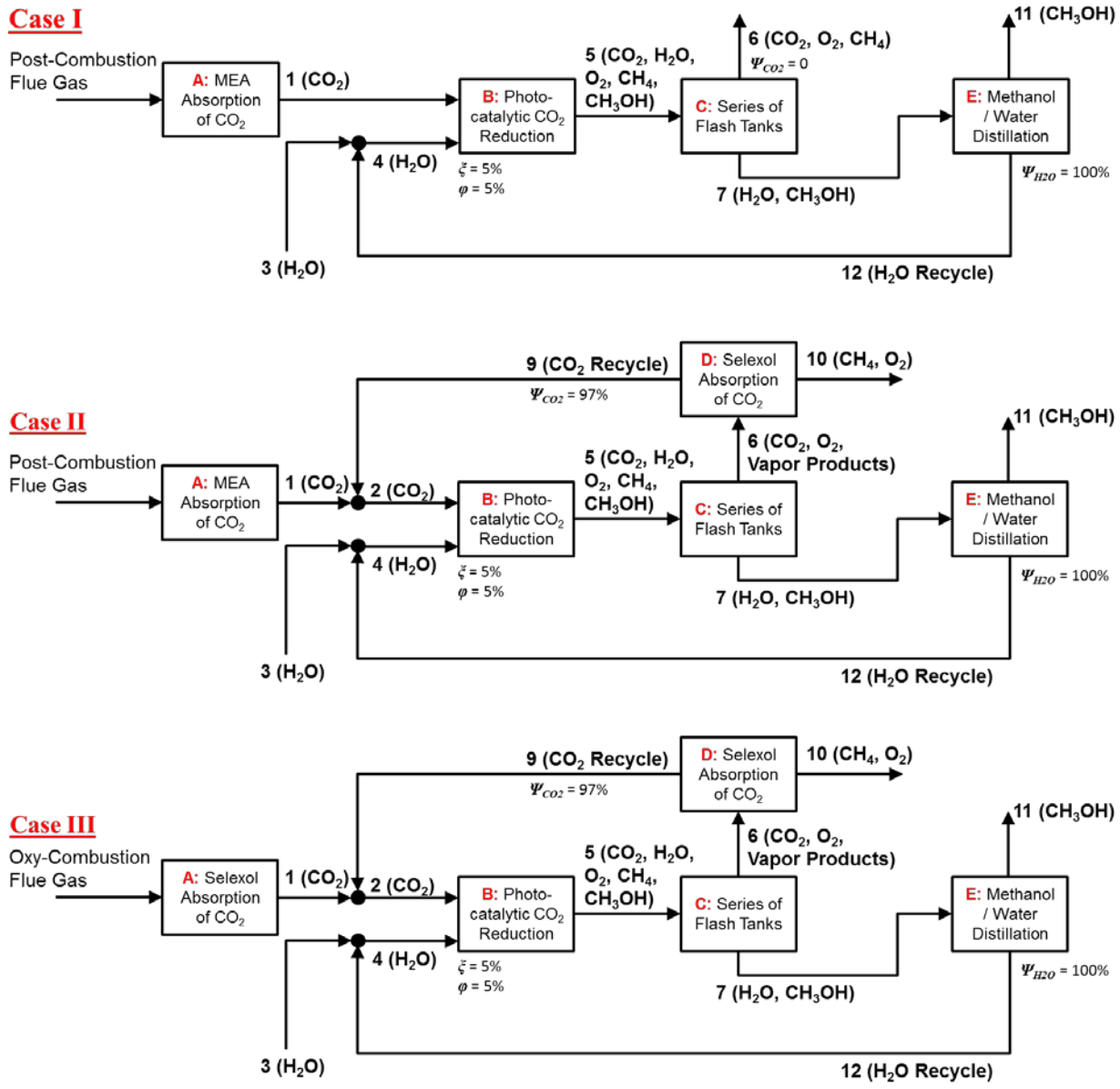

Figure S3. Block flow diagrams for direct CO_2 reduction to methanol and methane case studies.

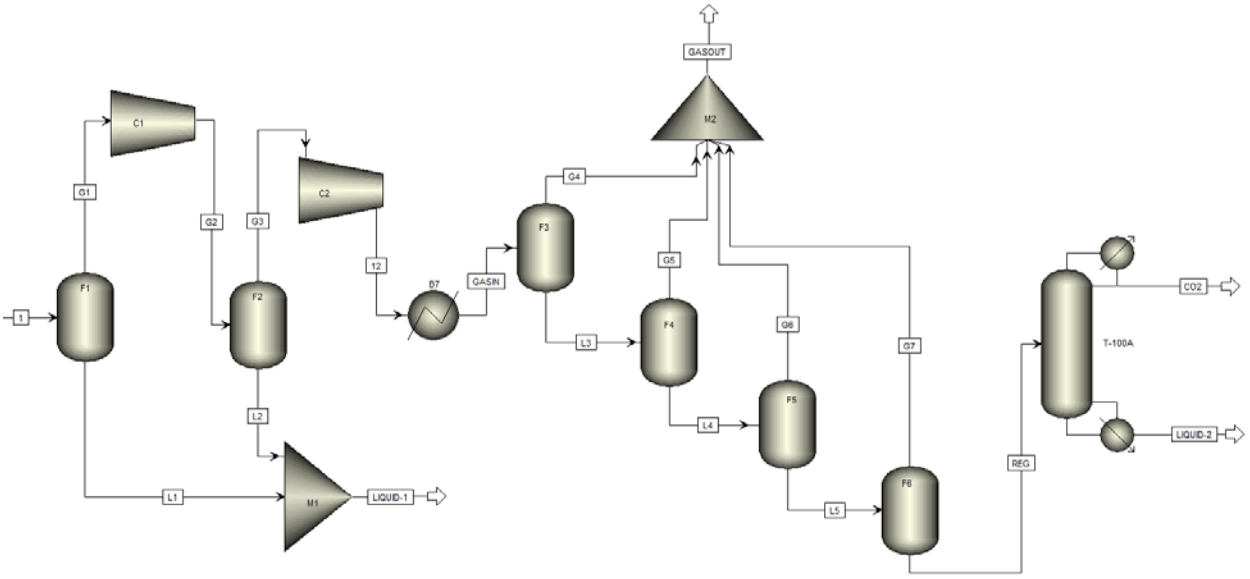

Figure S4. Process flow diagram for gas/liquid purification system. Light gases (CO_2, CH_4, and O_2) are separated from methanol/water stream.

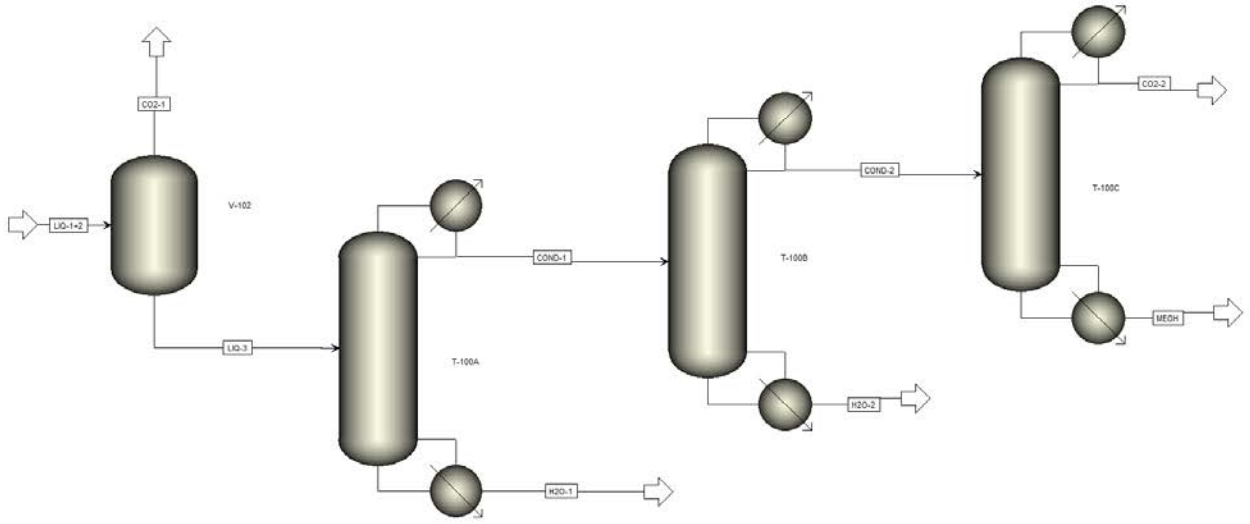

Figure S5. Process flow diagram for liquid product purification system (methanol, water, and residual CO_2 separation)

Sensitivity Analysis: CO_2 capture costs

In Figure S7, the energy incorporation efficiency as a function of CO2 one-pass conversion and specific CO2 capture costs. An analogous plot is presented in the main text (Figure 11). For reference, the specific CO_2 capture cost for our simulated MEA absorption process is 5.5 MJ kg_{CO2}^{-1}.

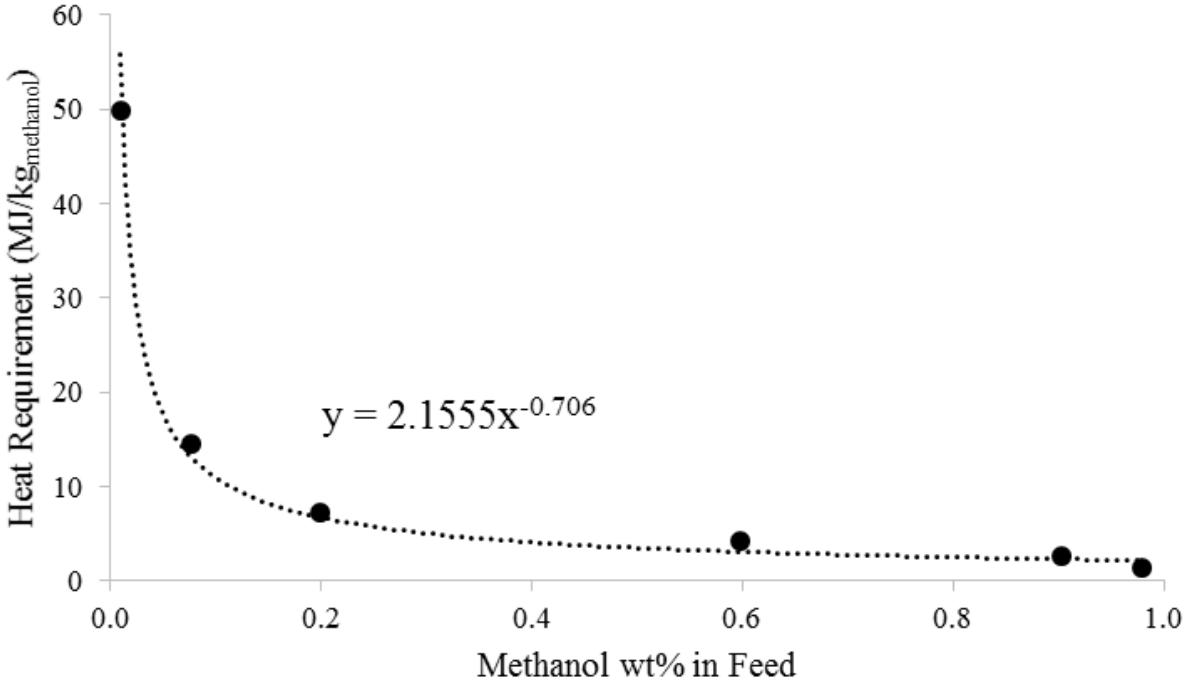

Figure S6. Calculated heating duty for Liquid Product Purification sub-system as function of methanol weight fraction incoming to system.

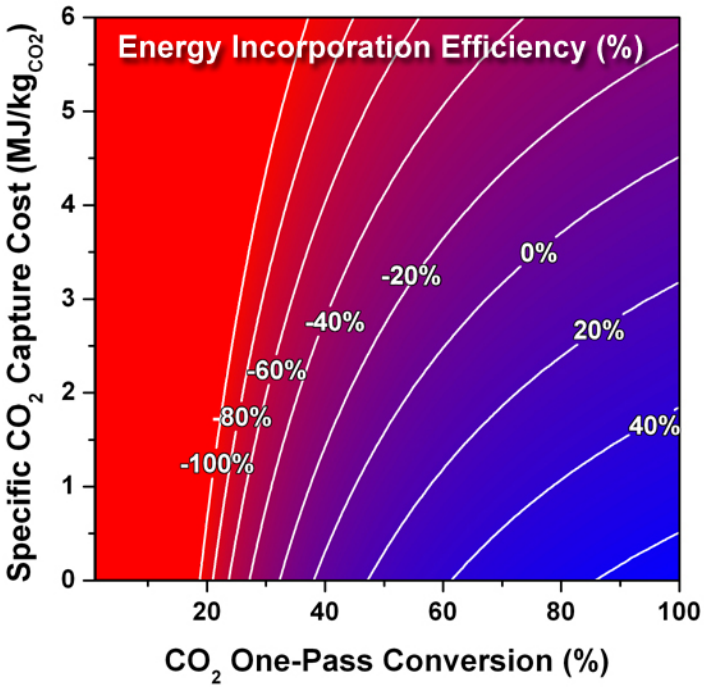

Figure S7. Energy incorporation efficiency for photo-catalytic reduction of CO_2 to methanol process for 1 kg/s methanol basis (22.7 MW HHV) as a function of CO_2 one-pass conversion and specific CO_2 capture cost, without including the value of methane produced. The domain is limited to (-100%, 100%) for clarity because the energy incorporation efficiency decreases rapidly at low conversion, obscuring the rest of the results.

Sensitivity Analysis: Improved selectivity versus by-product combustion

With 25% of the methane heating value utilized, the process can achieve positive energy incorporation efficiency with a specific CO_2 capture cost of 5.5 MJ kg^{-1} (the value we calculated for MEA absorption) at a one-pass conversion of 60%. If the specific CO_2 capture cost were reduced to 4.4 MJ kg^{-1}, a conversion of 51% would be required. In the case of an adsorption system, with a capture cost of 2 MJ kg^{-1}, 33% conversion would be required.

Since unwanted by-products can be combusted to recover process heating, how important is selectivity? The answer is not so clear. In the solar reactor, we are reducing CO_2 with H_2O to produce fuel (the opposite reaction of combustion) and so at first look, it seems obvious that the net effect should be zero. However, the CO_2 reduction reaction uses solar energy, and so there can be a "net primary energy gain." In the simple process we consider here, CO_2 is separated from O_2 and CH_4 in a single unit operation, leaving behind an O_2/CH_4 stream. With the base-case reaction stoichiometry, the ratio of CH_4:O_2 (1:3) is within the flammability limits (5-60 vol% in O_2) so it can be combusted to recover process heating without needing to dilute or remove excess oxygen. Though, if by-products require additional (or more costly) separation steps, there would be additional costs that would reduce the net amount of energy that can be recovered by combustion. Additionally, from a capital cost perspective, decreasing selectivity translates to increasing equipment size (and catalyst amounts) because the total mass flowing through the process would need to increase.

Economic Evaluation

Capital Costs

The total project investment was calculated by summing the direct and indirect capital costs. When the equipment cost was available (e.g. from direct Aspen simulation), the direct capital cost was calculated by multiplying the equipment cost by 2.3, to account for installation costs, instrumentation/control, piping, electrical systems, building (and services) and yard improvements. Otherwise, if the equipment cost was unavailable, the direct capital cost was taken directly from the source. In particular, the direct costs for the MEA-based[24] CO2 capture system and the Selexol[25] CO_2 separation system were taken from literature, while the equipment costs for the Gas/Liquid Separation and Liquid Product Purification systems were evaluated using Aspen Economic Analyzer.

Table S1. Direct capital costs and total capital investment (C_o) for sub-systems using the technology in the base-case scenario at a given capacity V_o. Please note that the value of V_o does not necessarily correspond to the mass flow rate through the base-case scenario.

Sub-System	Direct Capital Cost, C_o (USD)	Reference Volume, V_o (kg/s)
A: CO2 Capture & Transport	7,622,700	4.44
B: CO2 Reduction	*	1*
C: Gas/Liquid Separation	25,237,210	72.30
D: Gas Product Purification	19,280,498	24.84
E: Liquid Product Purification	685,170	56.30

* The capital costs for the solar reactor were not calculated and are left as a generic parameter for the sensitivity analysis.

By changing the process parameters (conversion, selectivity, etc.) the mass flow rates through the sub-systems changes and the direct capital cost is scaled with the following equation:

$$Direct\ Cost\ (USD) = C_o \left(\frac{V}{V_o}\right)^{0.67}$$

where C_o is the direct capital cost for the sub-system at a given mass flow rate (V_o) through the system, and V is the mass flow rate through the scaled system. The direct capital cost for the CO_2 capture system and Selexol system were scaled using only the CO_2 mass, while the other scenarios were scaled with respect to the total mass flowing through the system (as calculated using the generic mass balance).

The indirect capital cost was calculated by multiplying the direct capital cost by 0.5 to account for engineering, construction, legal/contractor fees, and project contingency. The total capital investment for each of the sub-systems was calculated by adding the direct and indirect costs.

All capital costs are scaled to a reference year of 2011 based on the Chemical Engineering Plant Cost Index (CEPCI).

Operating Costs

The fixed operating costs were estimated as a percentage of the direct capital costs as shown in Table S2.

Table S2. Fixed operating costs as function of capital costs

Labor Charge	2% of Direct Capital Cost
Overhead	60% of Labor Charge
Maintenance	3% of Direct Capital Cost
General & Administrative	5% of Direct Capital Cost
Tax & Insurance	2% of Total Capital Cost

Utilities costs and energy efficiency

The energy efficiency values and prices used in the analysis are based on literature values. Conventional resources to electricity efficiency (η_E) ranges from 32-38% depending on the fuel mixture and we assume a value of 37% based on the following energy mixture (US 2011): coal (41%), natural gas (25%), nuclear (21%), petroleum (1%), and renewable (12%).[26] Natural gas to heat efficiency (η_H) varies from 85-90%, and we assume a value of 86%. If the process energy were provided by solar utilities, we calculate the solar energy required by assuming a 45% solar energy to process heat conversion efficiency[27] and a 16% solar energy to electricity conversion efficiency (typical for crystalline silicon).[28]

The reported, average levelized costs for PV and CSP electricity are 144.3 USD MWh^{-1} and 261.3 USD MWh^{-1}, respectively.[29] The U.S. EIA has tabulated average electricity prices for the industrial sector (based on location), which we use as the basis for our price of 0.06 USD kWh^{-1}.[30]

CO_2 Reduction to methanol sensitivity

We calculated the minimum selling price of the base-case CO_2 reduction system as a function of methanol selectivity and CO_2 one-pass conversion (presented in the main text). In Figure S8, we show the total process energy consumption for those scenarios. The contribution of these energy costs towards the minimum selling price are shown in Figure S9a and Figure S9b. In Figure S9c, the contribution of the total capital investment and return on investment (ROI) towards the minimum selling price of methanol is shown.

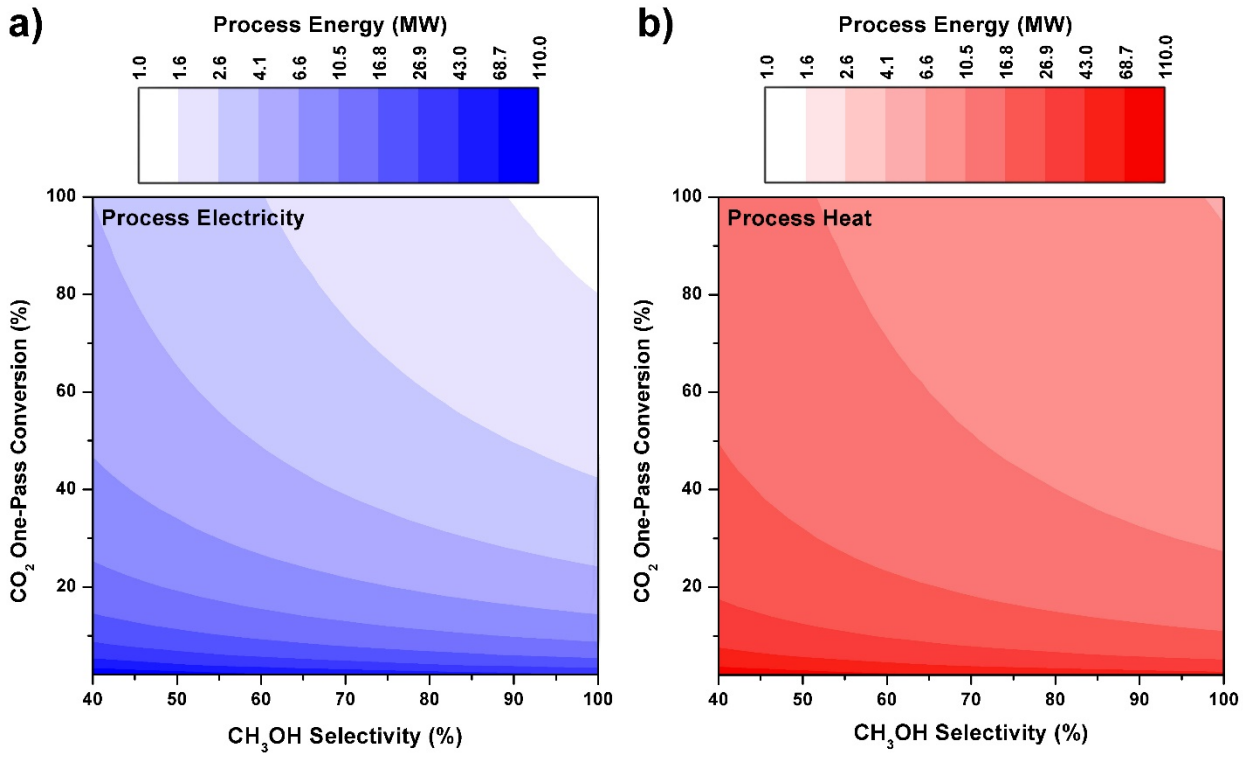

Figure S8. In a) process electricity consumption and b) process heat consumption for base-case CO_2 reduction process as function of methanol selectivity and CO_2 one-pass conversion.

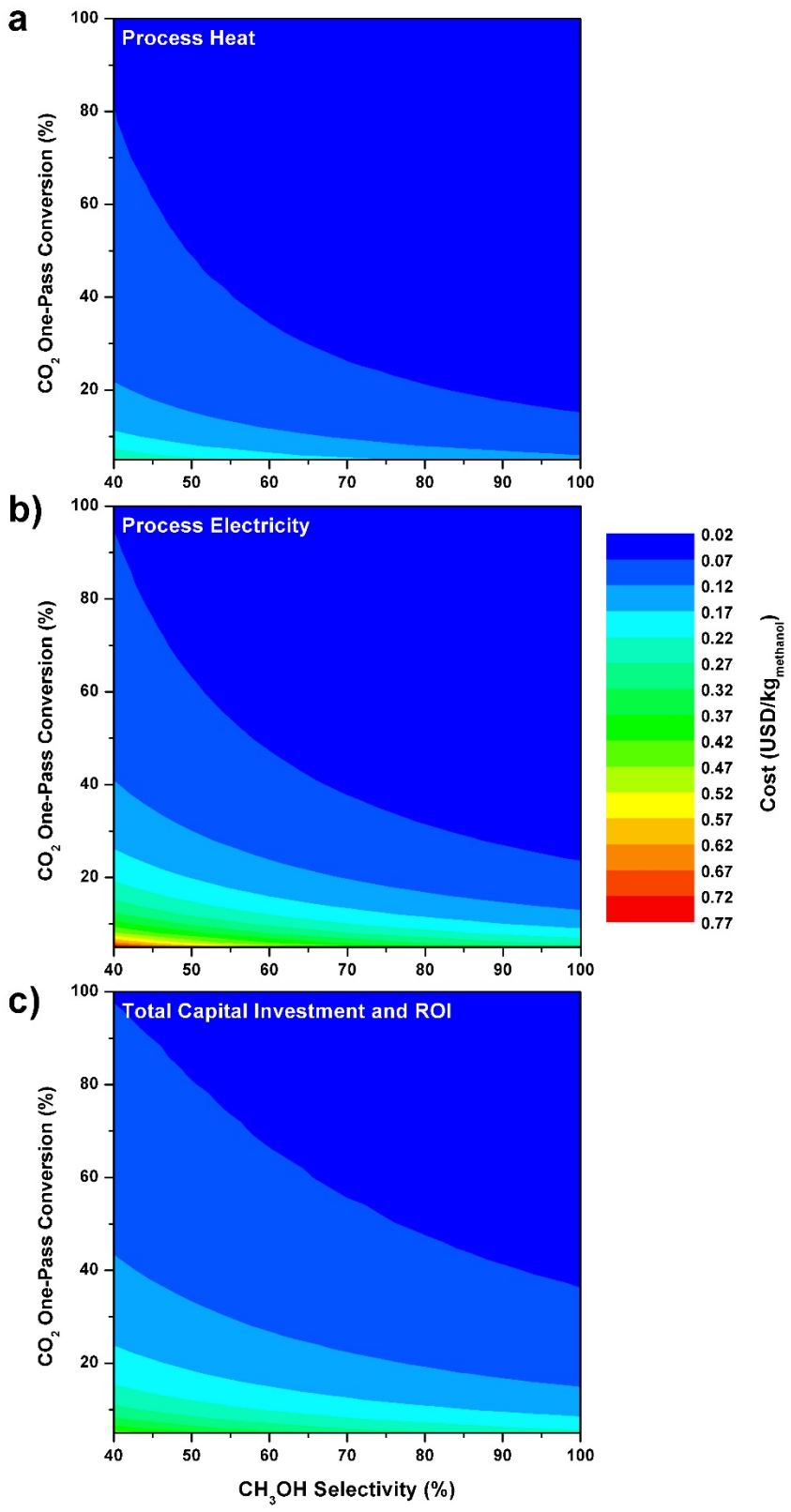

Figure S9. Contributions to minimum selling price for base-case CO_2 reduction process as function of methanol selectivity and CO_2 one-pass conversion. In a) contribution from process heating (all derived from fossil fuels), in b) contribution from process electricity (all derived from fossil fuel) and c) total capital investment and return on investment (ROI).

Solar Utilities versus fossil fuel utilities

The question is, what is the best strategy for replacing fossil utilities with solar utilities? First, we consider the price of the utilities. In our original economic analysis, we used fossil fuel utilities prices of 0.060 USD kWh^{-1} for electricity and 10.50 USD MT^{-1} (~0.017 USD kWh^{-1}) for process steam. In comparison, the levelized cost of solar-PV electricity has been studied quite extensively, and we will assume a value 0.144 USD kWh^{-1}.[29] In contrast, the cost of solar process heating has not been studied as extensively, we will use a literature value of 0.05 € kWh^{-1} (0.069 USD kWh^{-1} assuming a 1.38 USD to 1€ exchange rate).[31] Considering these prices, it would seem that the most economically efficient scenario would be to first replace fossil fuel heating with solar heating because the cost differential (cost of solar-derived heat – cost of fossil fuel-derived heat) is only 0.051 USD kWh^{-1}, whereas the cost differential for process electricity is 0.084 USD kWh^{-1}. However, what we really want to quantify is the cost of avoiding fossil fuel utilization. Importantly, when we replace 1 unit of fossil-fuel derived process utilities, the amount of primary (fossil fuel) energy avoided is a function of the fossil fuel to utilities conversion efficiency. In our analysis, we have assumed fossil fuels to process heating efficiency (η_H) of 86% and fossil fuels to electricity efficiency (η_E) of 37%. Therefore, for every 1 unit of fossil fuel electricity replaced with solar electricity, 2.7 units of primary energy are avoided. For fossil fuel heating, 1 unit of solar process heat avoids only 1.16 units of primary energy. As such, the true cost to avoid primary energy consumption is 0.031 USD kWh^{-1} if solar electricity is used, while the cost is 0.044 USD kWh^{-1} when solar heating is used. Therefore, for the numbers assumed here, it is always most economically efficient to replace fossil fuel-derived electricity with solar electricity rather than fossil fuel-derived heating with solar heating.

References

1. A. E. Cassano, C. A. Martin, R. J. Brandi and O. M. Alfano, *Ind. Eng. Chem. Res.*, 1995, **34**, 2155-2201.
2. R. J. Braham and A. T. Harris, *Ind. Eng. Chem. Res.*, 2009, **48**, 8890-8905.
3. H. Jin, Z. Wang, D. Zheng, Z. Hou, J. Sui and H. Hong, *Journal of Solar Energy Engineering*, 2007, **129**, 378-381.
4. M. van Well, V. W. Benz, M. A. Mueller, R. H. G. Dillert and D. W. Bahnemann, *Journal of Solar Energy Engineering*, 1997, **119**, 114-119.
5. J. C. S. Wu, H.-M. Lin and C.-L. Lai, *Applied Catalysis A: General*, 2005, **296**, 194-200.
6. T. Matsumura, D. Noshiroya, M. Tokumura, H. T. Znad and Y. Kawase, *Ind. Eng. Chem. Res.*, 2007, **46**, 2637-2647.
7. R. V. Siriwardane, M. S. Shen, E. P. Fisher and J. A. Poston, *Energy Fuels*, 2001, **15**, 279-284.
8. S. Keskin, T. M. van Heest and D. S. Sholl, *Chemsuschem*, 2010, **3**, 879-891.
9. J. R. Li, R. J. Kuppler and H. C. Zhou, *Chem. Soc. Rev.*, 2009, **38**, 1477-1504.
10. A. Phan, C. J. Doonan, F. J. Uribe-Romo, C. B. Knobler, M. O'Keeffe and O. M. Yaghi, *Acc. Chem. Res.*, 2010, **43**, 58-67.
11. C. W. Jones, *Annual Review of Chemical and Biomolecular Engineering, Vol 2*, 2011, **2**, 31-52.
12. J. C. Hicks, J. H. Drese, D. J. Fauth, M. L. Gray, G. G. Qi and C. W. Jones, *J. Am. Chem. Soc.*, 2008, **130**, 2902-2903.
13. X. C. Xu, C. S. Song, J. M. Andresen, B. G. Miller and A. W. Scaroni, *Energy Fuels*, 2002, **16**, 1463-1469.
14. Y. Belmabkhout and A. Sayari, *Adsorption*, 2009, **15**, 318-328.
15. P. J. E. Harlick and A. Sayari, *Ind. Eng. Chem. Res.*, 2007, **46**, 446-458.
16. T. Tsuda and T. Fujiwara, *J. Chem. Soc. Chem. Comm.*, 1992, 1659-1661.
17. J. H. Drese, S. Choi, R. P. Lively, W. J. Koros, D. J. Fauth, M. L. Gray and C. W. Jones, *Adv. Funct. Mater.*, 2009, **19**, 3821-3832.
18. E. J. Anthony, *Ind. Eng. Chem. Res.*, 2008, **47**, 1747-1754.
19. G. Grasa, B. GonzAlez, M. Alonso and J. C. Abanades, *Energy Fuels*, 2007, **21**, 3560-3562.
20. D. M. D'Alessandro, B. Smit and J. R. Long, *Angew. Chem. Int. Ed.*, 2010, **49**, 6058-6082.
21. A. Hanif, S. Dasgupta, S. Divekar, A. Arya, M. O. Garg and A. Nanoti, *Chem. Eng. J.*, 2014, **236**, 91-99.
22. *UOP Selexol Technology for Acid Gas Removal*, UOP LLC, 2009.
23. B. Burr and L. Lyddon, *A Comparison of Physical Solvents for Acid Gas Removal*, Bryan Research & Engineering, Inc.
24. J. Kim, T. A. Johnson, J. E. Miller, E. B. Stechel and C. T. Maravelias, *Energy Environ. Sci.*, 2012, **5**, 8417-8429.
25. C. Chen, Ph.D., Carnegie Mellon, 2005.
26. *Annual Energy Review 2011*, U.S. Energy Information Administration, 2011.
27. C. Perkins and A. W. Weimer, *AlChE J.*, 2009, **55**, 286-293.
28. *Solar Photovoltaic Cell/Module Shipments Report 2012*, U.S. Energy Information Administration, 2013.
29. *Annual Energy Outlook 2013*, U.S. Energy Information Administration Washington, DC, 2013.
30. *Electric Sales, Revenue, and average price*, U.S. Energy Information Administration, 2013.
31. R. Silva, M. Berenguel, M. Perez and A. Fernandez-Garcia, *Appl. Energy*, 2014, **113**, 603-614.